Journal of Materials Chemistry B

RSC Publishing

PAPER

View Article Online
View Journal | View Issue

Cite this: J. Mater. Chem. B, 2013, 1, 5806

Highly efficient "theranostics" system based on surface-modified gold nanocarriers for imaging and photodynamic therapy of cancer

Linlin Zhao,[a] Tae-Hyun Kim,[bc] Jin-Chul Ahn,[d] Hae-Won Kim[bc] and So Yeon Kim*[ae]

Nanoparticle technologies are significantly impacting the development of both therapeutic and diagnostic agents. At the intersection between treatment and diagnosis, interest has grown for combining both paradigms into clinically effective formulations. In this study we describe a highly efficient drug vector for photodynamic therapy (PDT) and cell imaging developed by designing multifunctional and biodegradable block copolymer–gold nanoparticle (AuNP) conjugates. These conjugates act as water-soluble and biocompatible carriers that allow the delivery of a hydrophobic photosensitizer to a tumor site for PDT action. The 17.6 nm citrate-stabilized AuNPs used herein were modified with folic acid (FA)-conjugated biocompatible block copolymers through a bidentate dihydrolipoic acid (DHLA) linker. The FA–PEG–P(Asp-Hyd)–DHLA-modified AuNPs (FA–PEG–P(Asp-Hyd)–DHLA–AuNPs) were sufficiently stable that their optical properties were not changed under very harsh conditions. Then, the hydrophobic photosensitizer, pheophorbide a (Pheo), was conjugated to the stable vectors through a pH-sensitive linkage. The synthesis and composition of all copolymers were confirmed by ^{1}H NMR measurement. The size of Pheo-conjugated FA–PEG–P(Asp-Hyd)–DHLA–AuNPs–Pheo determined by light-scattering measurements was about 54.7 nm. FE-SEM and FE-TEM images showed that these nanoparticles have a spherical shape and adequate dispersivity after modification. Confocal microscopy, flow cytometry assay, and bio-TEM measurements were used for determining the cellular uptake of Pheo and AuNPs in HeLa cells. The FA–PEG–P(Asp-Hyd)–DHLA–AuNPs–Pheo showed 99.16% cellular uptake and exhibited an excellent phototoxicity compared to free Pheo and FA-unconjugated nanoparticles at pH 6.4.

Received 4th July 2013
Accepted 2nd September 2013

DOI: 10.1039/c3tb20933d

www.rsc.org/MaterialsB

1. Introduction

For conventional cancer therapy methods, it is necessary to carry out diagnostic imaging to understand the cellular phenotype and heterogeneity of the tumor.[1,2] Inevitably, differences in biodistribution and selectivity are observed between distinct imaging and therapeutic agents. Since the new term "theranostic" was coined in 2002 by Funkhouser,[3] it has been increasingly recognized as a promising treatment for a variety of oncological, cardiovascular, dermatological, and ophthalmic diseases. A theranostic is defined as a material that combines the modalities of therapy and diagnostic imaging. Thus, theranostics deliver therapeutic drugs and diagnostic imaging agents at the same time within the same dose. The ultimate goal of the theranostic field is to gain the ability to image and monitor the diseased tissue, delivery kinetics, and drug efficacy with the long-term hope of gaining the ability to tune the therapy and dose with heretofore unattainable control.[4]

In this study, we developed a new theranostic system based on gold nanoparticles for photodynamic therapy (PDT). PDT is based on the use of photosensitizers (PS) that are preferentially taken up and retained by diseased tissue. Upon photoactivation with visible light at appropriate wavelengths, the generation of cytotoxic species such as reactive singlet oxygen ($^1O_2$) leads to irreversible destruction of tissues.[5–10] Compared to current treatments, including surgery, radiation therapy, and chemotherapy, PDT is an effective and selective method of destroying diseased tissue without damaging surrounding healthy tissues. PS are also ideal fluorescent markers for bioassays and cell imaging. However, a problem limiting the use of many current PS materials is the difficulty of preparing pharmaceutical formulations for parenteral administration. Because of their low water solubility, hydrophobic PS cannot be directly injected intravenously. To overcome these problems, we employed biocompatible block copolymer-modified gold nanoparticles (AuNPs) as a drug carrier. AuNPs have been extensively applied

[a]Graduate School of Green Energy Technology, Chungnam National University, Daejeon 305-764, South Korea. E-mail: kimsy@cnu.ac.kr; Tel: +82 42 821 5892
[b]Department of Nanobiomedical Science and WCU Research Center, Dankook University, Cheonan 330-714, South Korea
[c]Institute of Tissue Regeneration Engineering (ITREN), Dankook University, Cheonan 330-714, South Korea
[d]Department of Biomedical Engineering, College of Medicine, Dankook University, Cheonan, 330-714, South Korea
[e]Department of Chemical Engineering Education, College of Education, Chungnam National University, Daejeon 305-764, South Korea

as a drug delivery system and in imaging uses because of their high surface area, low toxicity, tunable size and shape, and well-established surface chemistry.[11] AuNP-based drug carriers have a small and tunable size, while exhibiting thermodynamic and kinetic stability *in vivo*, a high drug-conjugating capacity, and good biocompatibility.[12] When systemically injected, they exhibit prolonged circulation, and avoid rapid renal clearance and unwanted uptake by the reticuloendothelial system (RES). This results in enhanced permeability and retention (EPR) in tumor tissues with defective vascular architecture.[13] While the AuNPs produced by conventional methods are stable over extended periods of time in a specific condition, macroscopic aggregation is observed when the conditions change. Biocompatible and biodegradable polyethylene glycol (PEG) and poly(β-benzyl-L-aspartate) (PBLA) have been approved for human intravenous application, which were conjugated with a bidentate dihydrolipoic acid (DHLA) that permits strong interactions with AuNPs and promotes their dispersion in aqueous solution.[14,15]

Smart drug carriers show a greater delivery specificity to target sites through active targeting. Folic acid (FA) has become an attractive candidate molecule for targeting cancer cells, because it is an essential vitamin for nucleotide base biosynthesis and is taken up in elevated quantities by proliferating cells. The receptor for FA is over expressed in many human cancers, including malignancies of the ovary, brain, kidney, breast, myeloid cells, and lung.[16–18] In addition, stimuli-responsive nanocarriers exhibit controlled release by reactions to stimuli, such as temperature or pH.[19–23] The interstitial fluid in tumors is known to have a lower pH (pH 6.75) than normal tissues (pH 7.23). In addition, nanoparticles internalized by endocytosis are found in the acidic environments of endosomes (pH 5.0–6.0) and lysosomes (pH 4.5–5.0).[24] If such environments accelerate the degradation of pH-sensitive nanoparticles, the conjugated drug will be released. Therefore, the application of pH-sensitive nanoparticles may overcome the intracellular barriers of endosomal or lysosomal membranes that prevent drugs from reaching their targets.

There have been several researches which focused on the PS-conjugated AuNPs for PDT.[25–27] However, a Au-based nanocarrier system including a PS which was chemically conjugated through pH-sensitive linkage has not been reported.

Here, we report a highly efficient drug vector for PDT and imaging developed by designing multifunctional and biodegradable block copolymer–AuNP conjugates, which act as water-soluble and biocompatible carriers that deliver hydrophobic PS to a tumor site for PDT action. The 17.6 nm citrate-stabilized AuNPs were modified with FA-conjugated biocompatible block copolymers through a bidentate DHLA linker. A derivative of chlorophyll a, pheophorbide a (Pheo), was used as a PS. Pheo was conjugated to the side chain of the core-forming segment *via* an acid-labile hydrazone bond that is stable at physiological pH (7.0–7.4), but degraded at the lower pH (4.0–6.0) of the endosomal/lysosomal compartments. The molecular weights and chemical compositions of the copolymers were determined by ^{1}H NMR. The particle size, size distribution, and morphology were determined by DLS, SEM, and TEM. The stability of AuNP-based carriers under very harsh conditions was investigated. *In vitro* cellular localization was investigated in HeLa cells by confocal microscopy, flow cytometry, and TEM. The phototoxicity of free Pheo and AuNP-based nanocarriers was also investigated.

2. Results and discussion

2.1. Synthesis and characterization of FA–PEG–PBLA-based copolymers

Based on the previously reported block copolymers,[28] we conjugated a bidentate dihydrolipoic acid as a linker that permits strong interactions with AuNPs. The synthesis procedure is illustrated in Fig. 1.

First, folic acid ligands were introduced to copolymers for tumor targeting by the reaction of the amino group of PEG-bis(amine) with the FA carboxyl group (Fig. 1(A)). Second, the FA–PEG–PBLA block copolymer was synthesized by ring-opening polymerization of β-benzyl-L-aspartate *N*-carboxy anhydride (BLA-NCA) using the end amino group of FA–PEG–NH_2 in a DMF–chloroform solvent system as an initiator (Fig. 1(B)). These synthesized copolymers were confirmed by ^{1}H NMR spectra. As shown in Fig. 2(A), the peak at about 3.5 ppm corresponded to the methylene proton of PEG, and the peaks at 6.5 ppm, 7.4 ppm, and 8.5 ppm belong to the protons of C_h, C_g, and C_i in FA, respectively. For FA–PEG–PBLA the peaks at 5.1 ppm and 7.3 ppm correspond to the methylene protons and the PBLA side chain benzyl group, respectively. The peak at 8.2 ppm belongs to secondary amine protons in the PBLA main chain. Third, the bidentate dihydrolipoic acid was conjugated to FA–PEG–PBLA by reaction of the FA–PEG–PBLA amino group with the carboxyl group of α-lipoic acid. Fourth, the benzyl groups of FA–PEG–PBLA–LA were removed by a simple reaction of hydrazine monohydrate with the benzyl groups of the FA–PEG–PBLA block copolymer. Hydrazine monohydrate has two active amino functional groups. If the amount of hydrazine added is not enough, all of the amino groups could participate in the reaction, and it could play the role of a cross-linker. So an excess of hydrazine monohydrate was used to avoid cross-linking or branching of the polymer. In order to obtain bidentate dihydrolipoic acid, sodium borohydride was used to open the ring of α-lipoic acid (Fig. 1(C)). The composition of FA–PEG–P(Asp-Hyd)–DHLA was confirmed by ^{1}H NMR spectroscopy (Fig. 2(B)). For FA–PEG–PBLA–LA, the peaks at 1 to 2 ppm belong to the protons of α-lipoic acid, while for FA–PEG–P(Asp-Hyd)–DHLA the peaks at 5.1 ppm and 7.3 ppm corresponding to the methylene protons and PBLA side chain benzyl group disappeared. However, peaks at 4.4 ppm and 9.2 ppm were present. The latter represents the protons of the hydrazide groups, and indicates that the benzyl groups were successfully substituted with hydrazide groups.

Fifth, to form the pH-sensitive cleavage linker, the Pheo was modified by using 4-hydroxy-2-butanone to introduce the ketone groups (Fig. 1(D)), which was confirmed by ^{1}H NMR analysis. As shown in Fig. 2(C), compared to the original Pheo, the peaks a, b, and c, which belong to the protons of methyl and methylene in 4-hydroxy-2-butanone, appeared at about 1 ppm. This result indicates that the ketone groups were successfully conjugated onto the Pheo.

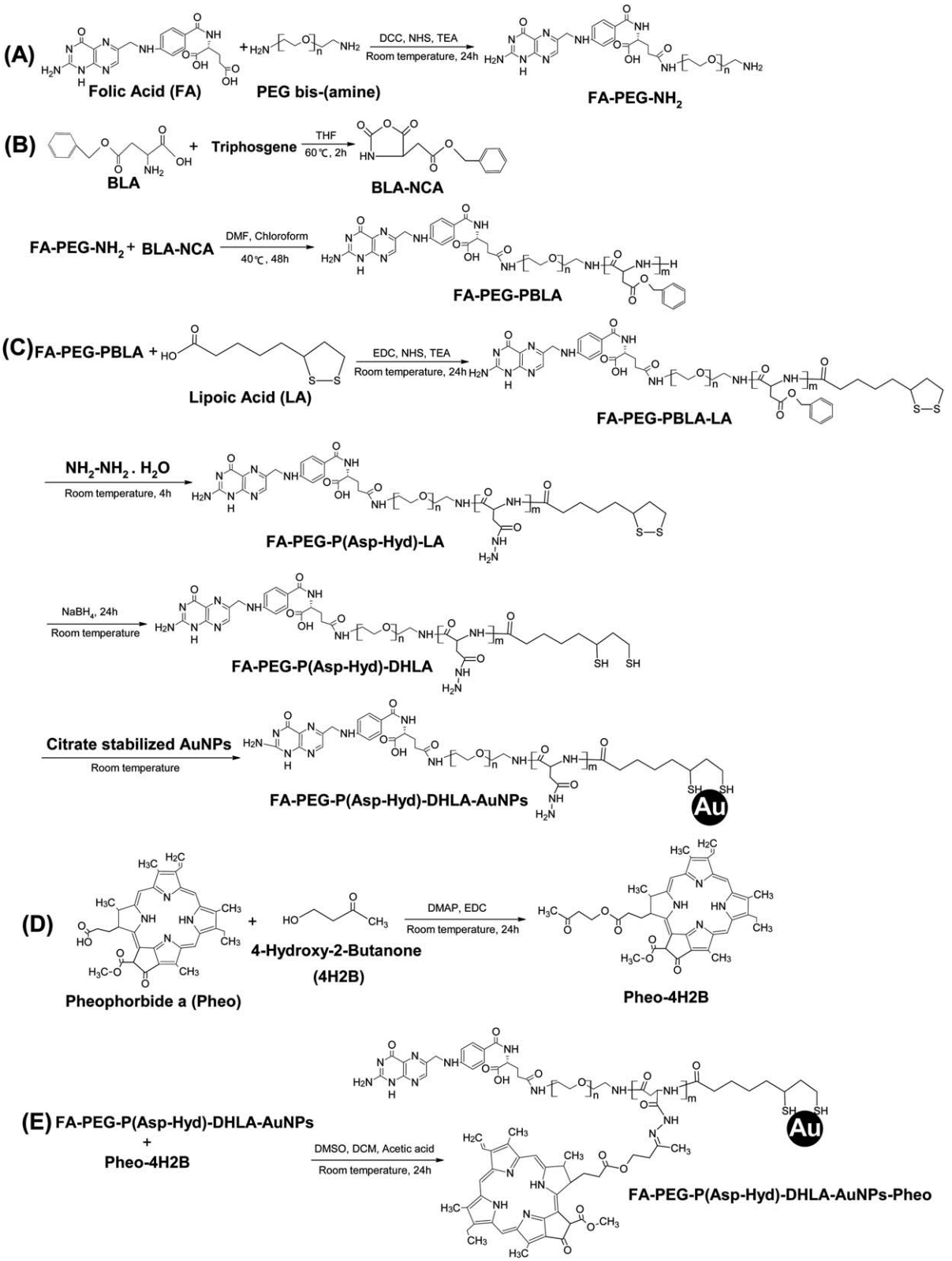

Fig. 1 Synthesis of (A) folic acid-conjugated PEG (FA–PEG–NH_2), (B) folic acid-conjugated amphiphilic PEG–PBLA copolymer (FA–PEG–PBLA), (C) FA–PEG–PBLA–LA, FA–PEG–P(Asp-Hyd)–LA, FA–PEG–P(Asp-Hyd)–DHLA, FA–PEG–P(Asp-Hyd)–DHLA–AuNPs, (D) modification of Pheo, and (E) FA–PEG–P(Asp-Hyd)–DHLA–AuNPs–Pheo.

In the final step, the modified Pheo was conjugated to the FA–PEG–P(Asp-Hyd)–DHLA–AuNPs through a pH-sensitive hydrazone linkage *via* an acetic acid-catalyzed reaction (Fig. 1(E)). Conjugation was confirmed by the presence of characteristic Pheo peaks at 8.8 ppm, 9.4 ppm, and 9.7 ppm, as well as characteristic peaks of FA, PEG, and PBLA (Fig. 2(D)).

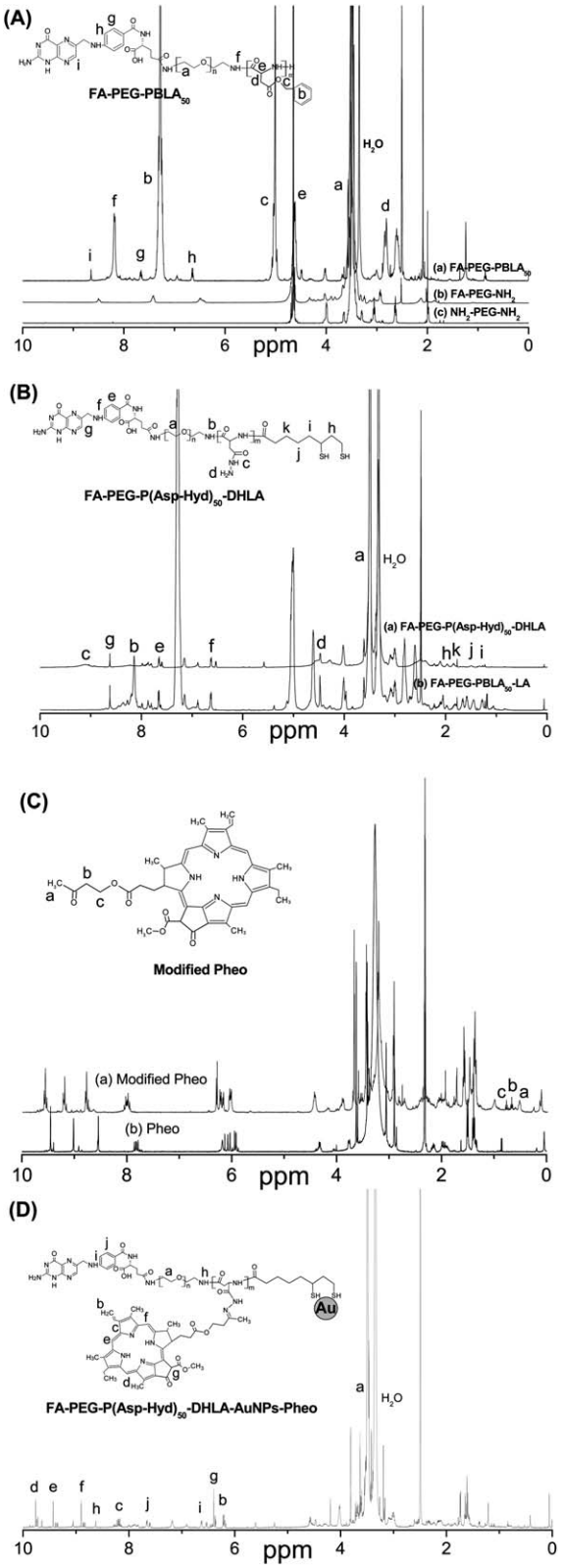

Fig. 2 ^{1}H NMR spectra of (A) FA–PEG–PBLA$_{50}$ (a), FA–PEG–NH$_2$ (b), NH$_2$–PEG–NH$_2$ (c); (B) FA–PEG–P(Asp-Hyd)$_{50}$–DHLA (a), FA–PEG–PBLA$_{50}$–LA (b); (C) modified Pheo (a), Pheo (b); and (D) FA–PEG–P(Asp-Hyd)$_{50}$–DHLA–AuNPs–Pheo.

The conjugation contents of Pheo to FA–PEG–P(Asp-Hyd)–DHLA–AuNPs were confirmed by ^{1}H NMR using the relative intensity ratio of the methylene protons of the PEG chain (–OCH$_2$CH$_2$–, 3.5 ppm) to the methane protons of Pheo (8.8 ppm, 9.4 ppm, and 9.7 ppm). The composition and properties of FA–PEG–P(Asp-Hyd)–DHLA–AuNPs–Pheo and CH$_3$–PEG–P(Asp-Hyd)–DHLA–AuNPs–Pheo are noted in Table 1. In this study, we selected FA–PEG–P(Asp-Hyd)$_{50}$–DHLA for further research, because the nanoparticle stability and drug-conjugation capability increased with increasing copolymer length.[28,29]

2.2. Confirmation of AuNP modification

The formation of AuNPs and the surface modification of AuNPs were confirmed by UV-visible, FT-IR spectroscopy and X-ray photoelectron spectroscopy (XPS) measurements. As shown in Fig. 3(A), the UV-visible spectra showed AuNPs, FA–PEG–P(Asp-Hyd)$_{50}$–DHLA–AuNPs, and FA–PEG–P(Asp-Hyd)$_{50}$–DHLA–AuNPs–Pheo characteristic surface plasmon resonance (SPR) bands at 519, 526, and 528 nm, respectively. These results indicate the formation and existence of AuNPs. The significant red shift in SPR with peak broadening of FA–PEG–P(Asp-Hyd)$_{50}$–DHLA–AuNPs and FA–PEG–P(Asp-Hyd)$_{50}$–DHLA–AuNPs–Pheo compared to the AuNPs suggests a linear increase in particle size consequent to the surface modification. The peak at 279 nm belongs to FA, and peaks at 379 nm and 686 nm belong to Pheo, respectively.

FT-IR measurements are shown in Fig. 3(B); the spectra of modified AuNPs exhibit a sharp band at 2883 cm^{-1}, which is attributed to the "C–H" stretch of FA–PEG–P(Asp-Hyd)$_{50}$–DHLA used for modification. Furthermore, some other bands at 1608 cm^{-1} and 1545 cm^{-1}, which were not present in the spectra of AuNPs, belong to amide groups of the copolymers.

In addition, XPS was employed to investigate the elemental compositions of the surface layer for AuNPs (Fig. 3(C)). For citrate-stabilized AuNP sample, Na, C, O, Si, and Au elements were clearly found. The signal corresponding to Si comes from the silicon wafer ((a) of Fig. 3(C)). After the modification of FA–PEG–P(Asp-Hyd)–DHLA polymeric ligands onto the surface of citrate-stabilized AuNPs by a ligand cap exchange method, two new peaks (a strong N absorption peak and a slight S absorption peak) appeared and the strong Na absorption peak disappeared ((b) and (c) of Fig. 3(C)). These results indicated that the FA–PEG–P(Asp-Hyd)$_{50}$–DHLA layer was successfully substituted onto the surface of AuNPs.

2.3. Stability of Au-based nanoparticles

In this study, we used a citrate-mediated reduction method to prepare AuNPs. After the reaction, the citrate ions attach to the surface of AuNPs and form a protective layer with a negative charge. Due to electrostatic repulsion, the AuNPs dispersed very well in solution. However, if the surrounding solution environment was changed, the charge balance would be undermined resulting in AuNP aggregation. However, after modification with FA–PEG–P(Asp-Hyd)$_{50}$–DHLA copolymers, the AuNPs could stably exist in solution under various harsh environments due to the steric repulsion of FA–PEG–P(Asp-Hyd)$_{50}$–DHLA copolymers.

Table 1 Characterization of Au-based nanoparticles

Samples[a]	Feed ratio[b] (molar ratio)	Copolymer composition[c] (molar ratio)	Molecular weight of polymer[d] (g mol^{-1})	Molar feed ratio (polymer : AuNPs)[e]	Size[f] (nm)	Polydispersity index[f]	DCC[g] (%)
FA–PEG–P(Asp-Hyd)$_{20}$–DHLA–AuNPs–Pheo	1 : 20	1 : 19.5	6513.2	2.5×10^4 : 1	51.1 ± 1.8	0.187 ± 0.021	10.9
FA–PEG–P(Asp-Hyd)$_{50}$–DHLA–AuNPs–Pheo	1 : 50	1 : 50.0	10 447.4		54.7 ± 1.2	0.151 ± 0.008	11.2
CH_3–PEG–P(Asp-Hyd)$_{50}$–DHLA–AuNPs–Pheo	1 : 50	1 : 48.8	9866.2		61.6 ± 1.6	0.179 ± 0.011	10.3

[a] FA/CH_3–PEG–P(Asp-Hyd)$_n$–DHLA–AuNPs–Pheo, n: number of BLA units. [b] The molar feed ratio of FA–PEG–NH_2 to BLA-NCA. [c] Molar composition of the copolymer, determined by ^{1}H NMR with DMSO-d_6 as a solvent (PEG to BLA units). [d] Molecular weight of FA/CH_3–PEG–P(Asp-Hyd)$_n$–DHLA, determined by ^{1}H NMR with DMSO-d_6 as a solvent. [e] Molar feed ratio of FA/CH_3–PEG–P(Asp-Hyd)$_n$–DHLA to citrate-stabilized AuNPs. (The size of citrate-stabilized AuNPs is 17.6 nm; concentration is 1.98×10^{-9} mmol ml^{-1}.) [f] Determined by DLS. [g] Drug conjugation content (DCC), determined by ^{1}H NMR using DMSO-d_6 as a solvent. $\mathrm{DCC}(\%) = \frac{\text{Amount of Pheo in nanoparticles}}{\text{Amount of Pheo loaded nanoparticles}} \times 100\% = \frac{\text{Pheo}}{\text{Pheo} + \text{Copolymer}} \times 100\%$.

The stability of AuNPs and FA–PEG–P(Asp-Hyd)$_{50}$–DHLA–AuNPs under various conditions was tested. As shown in Fig. 4(A) for the citrate-stabilized AuNPs, after mixing with 0.1 M NaOH, PBS, or dialysis against water, the solution color darkened, some precipitates were observed on the bottom of the vial, and the UV-visible absorption spectra also changed. However, the FA–PEG–P(Asp-Hyd)$_{50}$–DHLA copolymer-modified AuNPs demonstrated no change to the citrate-stabilized AuNPs, and could be stably stored over three months at room temperature. Fig. 4(B) demonstrates the stability of AuNPs under various pH conditions. We used acetic acid and NaOH solutions to adjust the pH, for citrate-stabilized AuNPs. After adding a drop of acetic acid or NaOH solution, the color and optical properties were significantly changed, while the FA–PEG–P(Asp-Hyd)$_{50}$–DHLA copolymer-modified AuNPs did not show significant changes. The FA–PEG–P(Asp-Hyd)$_{50}$–DHLA copolymer modification on the surface of AuNPs offers a great deal of flexibility in using AuNPs for biological applications where harsh conditions are ubiquitous; for example, many cellular organelles are maintained at acidic conditions and are rich in dissolved ions.

2.4. Morphology of Au-based nanoparticles

For nanocarriers used in cancer therapy, size, morphology, and stability are the key properties that influence *in vivo* performance. These factors affect the biodistribution and circulation time of the drug carriers. Stable and smaller particles have reduced uptake by the RES and provide efficient passive tumor-targeting ability *via* an EPR effect.[30]

The citrate-mediated reduction method could be used to prepare spherical AuNPs, and the modification of the FA–PEG–P(Asp-Hyd)$_{50}$–DHLA copolymer could promote their stability. We examined the size, size distribution, and morphology of citrate-stabilized AuNPs, FA–PEG–P(Asp-Hyd)$_{50}$–DHLA–AuNPs, and Pheo-conjugated FA–PEG–P(Asp-Hyd)$_{50}$–DHLA–AuNPs–Pheo by DLS, FE-SEM, and FE-TEM.

Fig. 5 shows the typical size distribution of citrate-stabilized AuNPs, FA–PEG–P(Asp-Hyd)$_{50}$–DHLA–AuNPs, FA–PEG–P(Asp-Hyd)$_{50}$–DHLA–AuNPs–Pheo, and CH_3–PEG–P(Asp-Hyd)$_{50}$–DHLA–AuNPs–Pheo. DLS measurements showed average sizes of 17.6, 51.2, 54.7, and 61.6 nm, respectively. After the surface modification of AuNPs, the size increased somewhat (about 33–44 nm) due to the presence of a fairly thick copolymer layer on the surface of AuNPs. However, the size distribution maintained a narrow and monodisperse unimodal pattern (Fig. 5(B)–(D)).

The morphology of citrate-stabilized AuNPs, FA–PEG–P(Asp-Hyd)$_{50}$–DHLA–AuNPs, and FA–PEG–P(Asp-Hyd)$_{50}$–DHLA–AuNPs–Pheo was evaluated by FE-SEM and FE-TEM (Fig. 6). The nanoparticles were submicron in size and nearly spherical with no aggregation between nanoparticles observed. Although the nanoparticles aggregate due to surface tension as the water evaporates during sample preparation, the modified AuNP cores do not coalesce and fuse. The mean diameter and size distribution of these nanoparticles are similar to those of citrate-stabilized AuNPs, which indicate that the integrity of AuNPs was not affected by FA–PEG–P(Asp-Hyd)$_{50}$–DHLA modification. In addition, because of the FA–PEG–P(Asp-Hyd)$_{50}$–DHLA modification, the dispersibility of nanoparticles improved compared to the citrate-stabilized AuNPs, as shown in Fig. 6.

2.5. Cellular uptake of Pheo-conjugated AuNPs

The efficiency of PDT treatment is highly dependent on the cellular uptake of the PS and its accumulation in malignant tissues.[31] The intracellular localization of free Pheo, CH_3–PEG–P(Asp-Hyd)$_{50}$–DHLA–AuNPs–Pheo, and FA–PEG–P(Asp-Hyd)$_{50}$–DHLA–AuNPs–Pheo in HeLa cells was investigated using confocal laser scanning microscopy and flow cytometry.

The confocal microscopy assay was based on the red autofluorescence of Pheo, the blue fluorescence from DAPI bound to the nucleus, and F-actin in the cytoplasm stained by Alexa Fluor 488 phalloidin (Fig. 7(A)). When HeLa cells were incubated with free Pheo, CH_3–PEG–P(Asp-Hyd)$_{50}$–DHLA–AuNPs–Pheo, and FA–PEG–P(Asp-Hyd)$_{50}$–DHLA–AuNPs–Pheo for 4 h, they showed a similar cellular localization of Pheo molecules. The HeLa cell samples treated with free Pheo, CH_3–PEG–P(Asp-Hyd)$_{50}$–DHLA–AuNPs–Pheo, and FA–PEG–P(Asp-Hyd)$_{50}$–DHLA–AuNPs–Pheo produced strong fluorescence signals from Pheo around the nucleus and at the inner part of the cells, indicating that Pheo

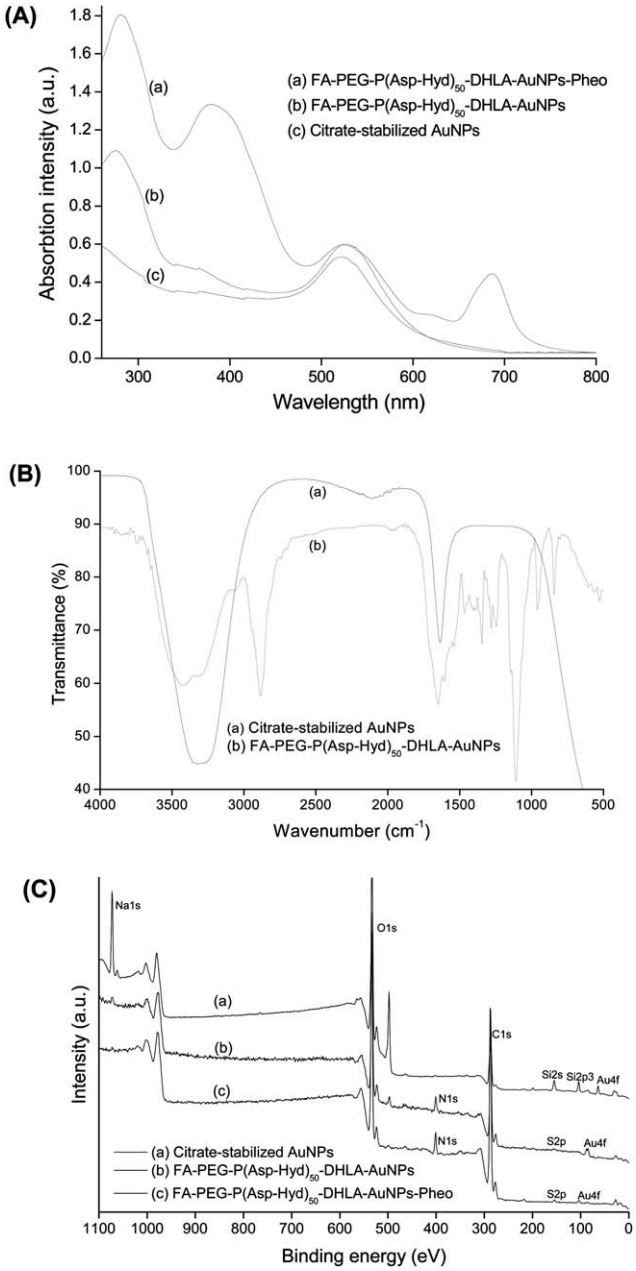

Fig. 3 (A) UV-visible absorption spectra, (B) FT-IR spectra and (C) XPS spectra used to confirm the modification of AuNPs.

molecules were internalized into the nucleus. These strong fluorescence signals from Pheo and the nucleus could be used for clearly understanding the dynamics of intracellular networks, and signal transduction in diagnostics. In addition, the flow cytometry assay showed relatively high cellular uptake (>90%) in all samples, as shown in Fig. 7(B), which is probably due to the slightly higher water solubility of Pheo (about 15 μg ml^{-1}) compared to other hydrophobic PSs (*e.g.*,2,4-diacetyl deuteroporphyrin IX dimethyl ether, water insoluble[28]). However, after incubation of FA–PEG–P(Asp-Hyd)$_{50}$–DHLA–AuNPs–Pheo with HeLa cells for 4 h, the cellular uptake of Pheo molecules was about 99.16%, which was slightly higher than that of free Pheo (97.63%) and CH_3–PEG–P(Asp-Hyd)$_{50}$–DHLA–AuNPs–Pheo

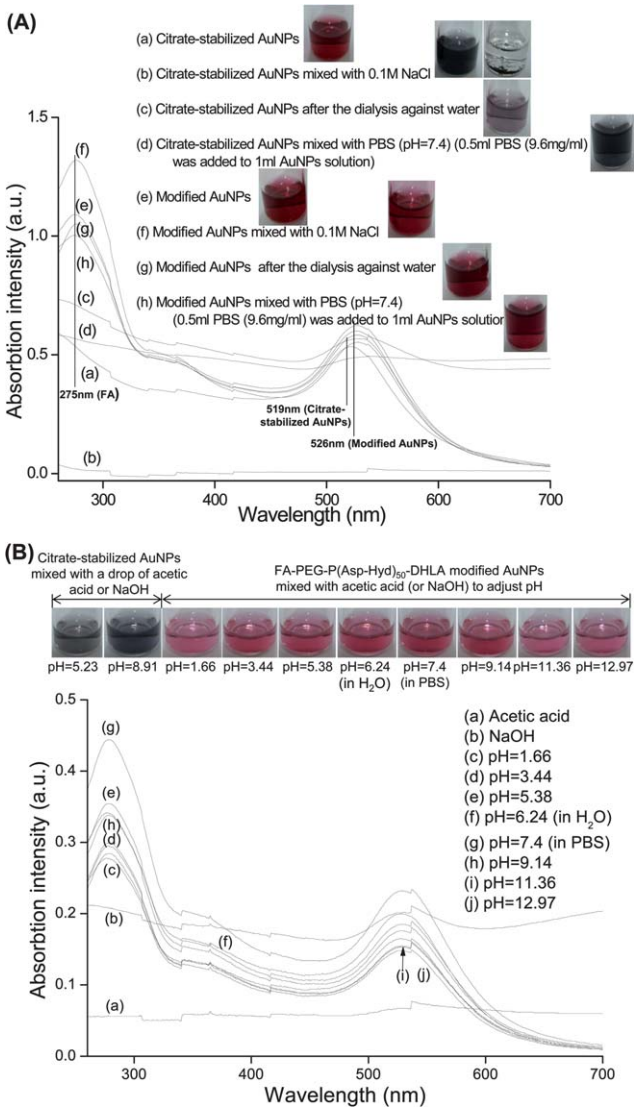

Fig. 4 Stability of citrate-stabilized AuNPs and FA–PEG–P(Asp-Hyd)$_{50}$–DHLA modified AuNPs investigated by UV-visible absorption spectra and images (A) under high ion concentration and (B) under various pH values.

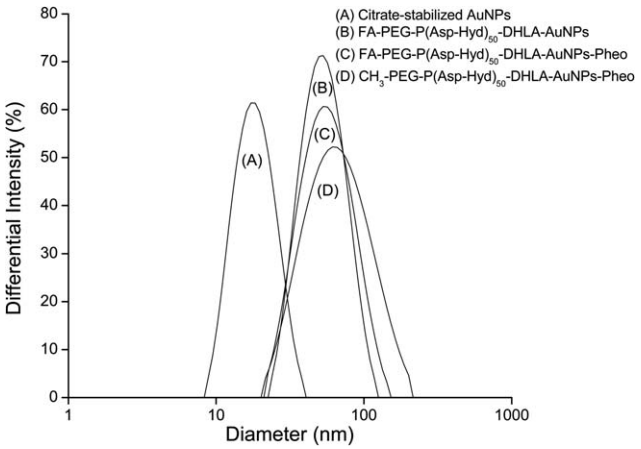

Fig. 5 Typical size distributions of (A) citrate-stabilized AuNPs, (B) FA–PEG–P(Asp-Hyd)$_{50}$–DHLA–AuNPs, (C) FA–PEG–P(Asp-Hyd)$_{50}$–DHLA–AuNPs–Pheo, and (D) CH_3–PEG–P(Asp-Hyd)$_{50}$–DHLA–AuNPs–Pheo.

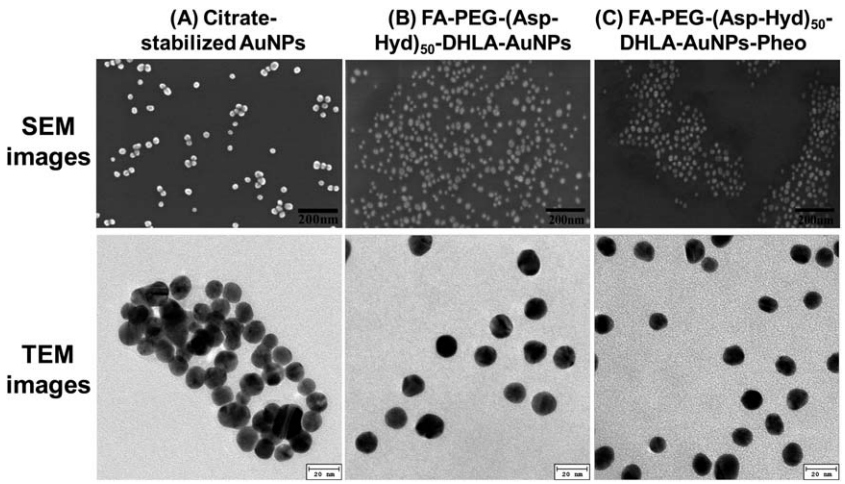

Fig. 6 FE-SEM and FE-TEM images of (A) citrate-stabilized AuNPs, (B) FA–PEG–P(Asp-Hyd)$_{50}$–DHLA–AuNPs, and (C) FA–PEG–P(Asp-Hyd)$_{50}$–DHLA–AuNPs–Pheo.

(97.80%). This result could be due to the conjugation of FA ligands, which promoted the cellular uptake of FA–PEG–P(Asp-Hyd)$_{50}$–DHLA–AuNPs–Pheo.

2.6. Cellular localization of AuNPs in HeLa cells

The modified AuNPs have shown minimal protein adsorption and little or no uptake in cancer cells' nuclei, except when a special targeting ligand is present.[25,29,32] Because of the insufficient cellular uptake of AuNPs, as demonstrated in previous studies,[25,29,32] to increase the probability of detecting AuNPs by TEM, we increased the concentration of AuNPs by more than ten-fold compared to prior Pheo cellular uptake tests for the TEM monitoring experiment. After 24 h of incubation with the AuNP-based nanoparticles, only a few AuNPs were found freely dispersed in the cells, and they were treated as intruders and confined in the endosome, as shown in Fig. 8(A) and (B).[32,33] Due to the weakly acidic condition of the endosome and lysosome, the Pheo was released from the FA–PEG–P(Asp-Hyd)$_{50}$–DHLA–AuNPs–Pheo and allowed to cross the endosomal or lysosomal membrane into the nucleus.[24] However, the AuNPs were well retained in the endosome until they were ejected from the cells. As shown in Fig. 8(C), some AuNPs could be found adjacent to the plasma membrane of the cells. These results indicated that the Pheo molecules, which were released in the endosomes or lysosomes and taken up by HeLa cells' nuclei, could not be

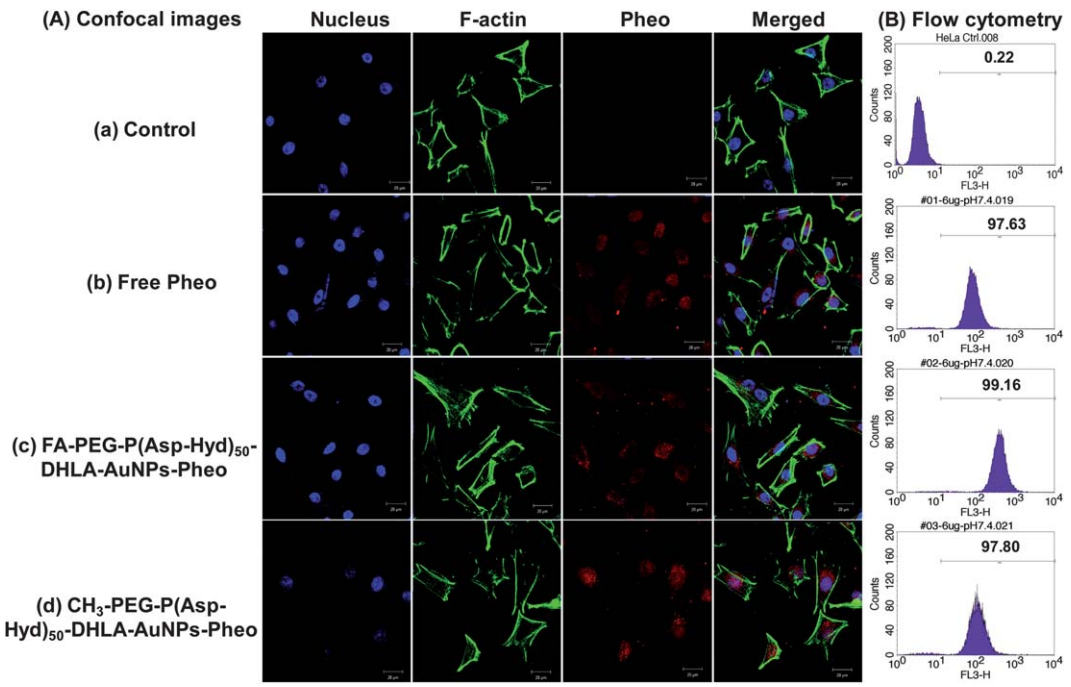

Fig. 7 (A) Confocal images and (B) flow cytometry assay results of cellular uptake of free Pheo, FA–PEG–P(Asp-Hyd)$_{50}$–DHLA–AuNPs–Pheo, and CH$_3$–PEG–P(Asp-Hyd)$_{50}$–DHLA–AuNPs–Pheo against HeLa cells [DAPI (blue); Alexa Fluor 488 Phalloidin (green), Pheo (red)]. Scale bars represent 20 μm.

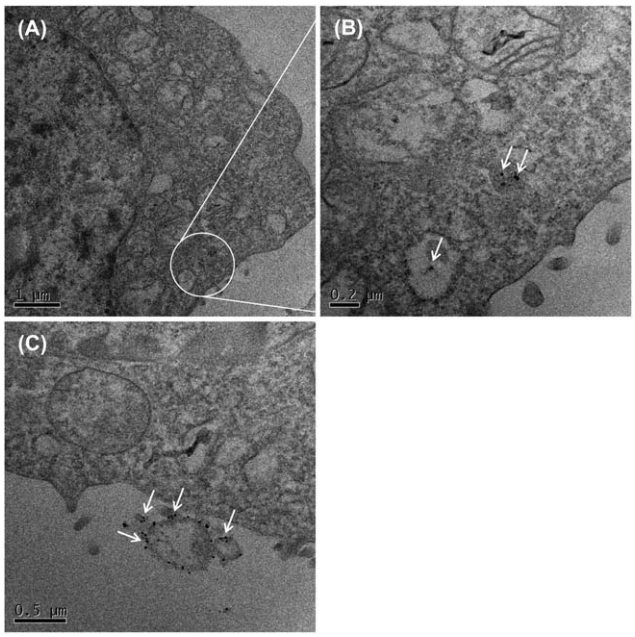

Fig. 8 TEM images of thin sections of HeLa cells after incubation with FA–PEG–P(Asp-Hyd)$_{50}$–DHLA–AuNPs–Pheo for 24 h. The arrows indicate the position of AuNPs.

quenched by AuNPs and did not influence their therapeutic efficiency. Nevertheless, the mechanisms of cellular uptake for AuNPs are not well understood and studies performed in different laboratories are sometimes inconsistent or even totally conflicting.[33] In future studies, we are planning to investigate the fate of FA–PEG–P(Asp-Hyd)$_{50}$–DHLA–AuNPs–Pheo in HeLa cells, as well as *in vivo* behaviors.

2.7. *In vitro* cytotoxicity test of Pheo-conjugated nanoparticles

To determine the PDT efficacy of Pheo-conjugated nanoparticles, the *in vitro* cytotoxicity of free Pheo and Pheo-conjugated nanoparticles was investigated by the CCK-8 assay and the average cell viability was monitored. In the dark toxicity test, the free Pheo and Pheo-conjugated nanoparticles exhibited no significant dark toxicity both at pH 6.4 and pH 7.4. As the concentration increased, the average cell viability showed a slight decrease due to the high concentration of AuNPs (Fig. 9(A)).[34,35] However, cell viability was greater than 73% when cells were treated with 20 μg ml^{-1} of Pheo.

For the phototoxicity test, we investigated using various laser exposure times (0, 15, and 30 min) and various Pheo concentrations (0, 3, 6, 10, 15, and 20 μg ml^{-1}). As shown in Fig. 9(B), when 10 μg ml^{-1} Pheo and 0.4 mW cm^{-2} laser intensity were used, the free Pheo, CH_3–PEG–P(Asp-Hyd)$_{50}$–DHLA–AuNPs–Pheo, and FA–PEG–P(Asp-Hyd)$_{50}$–DHLA–AuNPs–Pheo exhibited significantly enhanced phototoxicity compared to dark toxicity. The cell viability decreased drastically as laser exposure time increased, especially for FA–PEG–P(Asp-Hyd)$_{50}$–DHLA–AuNPs–Pheo, whose average cell viability was nearly 10% lower than that of the other materials. This result might be due to the enhanced cellular uptake by FA conjugation, which promoted phototoxicity.

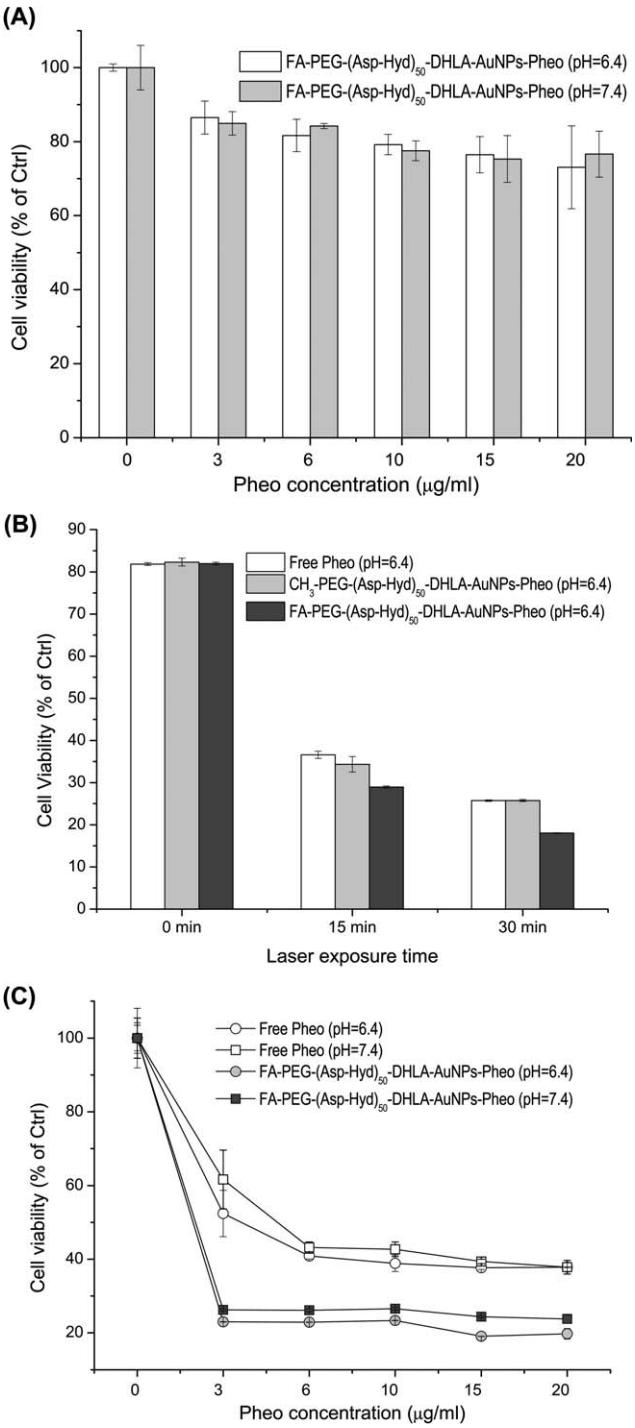

Fig. 9 *In vitro* cytotoxicity test using free Pheo, FA–PEG–P(Asp-Hyd)$_{50}$–DHLA–AuNPs–Pheo and CH_3–PEG–P(Asp-Hyd)$_{50}$–DHLA–AuNPs–Pheo against HeLa cells, (A) dark toxicity depending on Pheo concentration, (B) phototoxicity depending on laser exposure time, and (C) phototoxicity depending on Pheo concentration.

As shown in Fig. 9(C), after irradiation at 0.4 mW cm^{-2} for 10 min, the cell viability gradually decreased as the Pheo concentration increased. The efficiency of FA–PEG–P(Asp-Hyd)$_{50}$–DHLA–AuNPs–Pheo was obviously higher than that of free

Pheo. This is probably due to the nanoparticles improving the Pheo solubility in aqueous environments and increasing $^1O_2$ quantum yield.[36] In the case of FA–PEG–P(Asp-Hyd)$_{50}$–DHLA–AuNPs–Pheo, the cell viability at pH 6.4 was lower than that at pH 7.4. This could be due to the rapid release of Pheo from nanoparticles containing pH-sensitive hydrazone linkages.[24] Therefore, the phototoxicity effect of FA–PEG–P(Asp-Hyd)$_{50}$–DHLA–AuNPs–Pheo could be enhanced under weakly acidic extracellular conditions compared with that at physiological pH. This result suggests that FA–PEG–P(Asp-Hyd)$_{50}$–DHLA–AuNPs–Pheo is suitable for PDT in the weakly acidic conditions of tumor tissue.

3. Conclusions

To develop a novel efficient theranostic system, which provides excellent phototoxicity and cell imaging properties using the autofluorescence of PS, tumor-targeting, ligand-conjugated, multifunctional and biodegradable block copolymer–AuNP conjugates were designed as drug vectors. Their pH-sensitive release behaviors were used for targeting Pheo delivery for PDT and cell imaging. The FA–PEG–P(Asp-Hyd)$_{50}$–DHLA–modified AuNPs as drug carriers exhibit adequate stability under various harsh conditions. DLS, FE-SEM, and FE-TEM measurements indicated that these nanocarriers have a spherical shape and a narrow size distribution with a mean diameter of 54.7 nm. These stable nanoparticles are suitable for the EPR effect and circulation in the body. Due to the tumor-targeting ligand conjugation, cellular uptake and phototoxicity against HeLa cells were enhanced. These PS-conjugated and stabilized AuNPs containing tumor targeting FA ligands and pH-sensitive cleavage sites could improve the solubility of Pheo and increase $^1O_2$ quantum yield in the weakly acidic conditions of tumor tissue, as well as promote PDT treatment efficiency. In addition, this nanocarrier showed that strong fluorescence signals could aid in diagnostic imaging to understand the cellular phenotype. These results suggest that the FA–PEG–(Asp-Hyd)$_{50}$–DHLA-modified AuNP theranostic system has the potential as an effective PS delivery system for PDT applications and cell imaging.

4. Experimental section

4.1. Materials

α-Lipoic acid (LA), sodium citrate tribasic dihydrate, FA, PEG-bis(amine) (molecular weight: 3.350 kDa), β-benzyl-L-aspartate (BLA), triethylamine (TEA), hydrazine monohydrate, sodium bicarbonate, and *N*-(3-dimethylaminopropyl)-*N*′-ethyl-carbodiimide hydrochloride (EDC) were purchased from Sigma Chemical Co. (St Louis, MO, USA). Chloroauric acid, triphosgene, and 4-(dimethylamino) pyridine (DMAP) were purchased from Aldrich Chemical Co. (Milwaukee, WI, USA). Sodium borohydride, *N*-hydroxysuccinimide (NHS), and *N*,*N*′-dicyclohexylcarbodiimide (DCC) were purchased from Fluka (Buchs, Switzerland). 4-Hydroxy-2-butanone was purchased from TCI (Tokyo, Japan). Dimethyl sulfoxide (DMSO), tetrahydrofuran (THF), *n*-hexane, benzene, *N*,*N*-dimethylformamide (DMF), chloroform, diethyl ether, 1,4-dioxane, methanol, dichloromethane (DCM), and acetic acid were obtained from Samchun Pure Chemical Co., Ltd (Gyeonggi-do, Korea). Pheophorbide a (Pheo) was purchased from Frontier Scientific, Inc. (Logan, UT, USA). Spectra/Por membranes were purchased from Spectrum Laboratories, Inc. (Rancho Dominguez, CA, USA). RPMI 1640 medium, Dulbecco's modified Eagle's medium (DMEM), fetal bovine serum (FBS), penicillin, streptomycin, and Dulbecco's phosphate buffered saline (DPBS) were obtained from Gibco BRL (Invitrogen Corp., CA, USA). All other chemicals were analytical grade and used as received without further purification.

4.2. Synthesis of AuNP-based nanocarriers

4.2.1. Preparation of citrate-stabilized AuNPs. The synthesis of citrate-stabilized AuNPs was carried out according to the method of G. Frens.[37] 800 ml of 0.1 mg ml^{-1} chloroauric acid solution was stirred and heated to boiling in an oil bath, and 16 ml of 10 mg ml^{-1} sodium citrate tribasic dihydrate solution was then added. After this addition, the color of the boiling mixture solution changed from pale yellow to colorless, indicating the beginning of reduction. In the initial stage of the reaction, the solution color gradually changed from very dark blue to purple, and finally, wine red. When the wine red color appeared, boiling continued for at least 20 minutes in order to complete the reaction, followed by natural cooling to room temperature and storage in a refrigerator for future use. The concentration was determined by UV-vis spectra according to the method of W. Haiss.[38]

4.2.2. Synthesis of block copolymers for AuNP modification. For the surface modification of AuNPs, we used the FA-conjugated PEG–P(Asp-Hyd) block copolymer as previously reported.[28] Briefly, the copolymer for the surface modification of AuNPs was synthesized *via* several steps:

4.2.2.1. Synthesis of folic acid–PEG–NH$_2$ (FA–PEG–NH$_2$). FA (113 mg; 0.25 mmol) was dissolved completely in DMSO (6 ml), and NHS (37 mg; 0.32 mmol), *N*,*N*′-dicyclohexylcarbodiimide (66 mg; 0.32 mmol), PEG-bis(amine) (714.8 mg; 0.21 mmol), and TEA (170 μl; 2.1 mmol) were added. In order to obtain a mono-substitution of the amino group in the PEG-bis(amine) (FA–PEG–NH$_2$), we defined the molar feed ratio of FA to PEG-bis-(amine) at 1.2 : 1. The reaction mixture was stirred at 400 rpm for 24 h at room temperature in the dark under nitrogen. The mixture was diluted with 18 ml of deionized water and the by-product, dicyclohexylurea, was removed by filtration.[39–41] The product was purified by dialysis against a $NaHCO_3$ solution (pH 8.4) for 2 days to remove unconjugated FA, then dialyzed against deionized water to remove $NaHCO_3$, and finally freeze-dried.

4.2.2.2. Preparation of β-benzyl-L-aspartate N-carboxy anhydride (BLA-NCA). BLA (7.2 g; 32.3 mmol) was added to a round-bottom flask. Triphosgene (4.3 g; 14.5 mmol) dissolved in anhydrous THF (70 ml) was added slowly. The reaction mixture was stirred at 60 °C under nitrogen for 2 h. The mixture became clear during the reaction. The solvent of the reactant mixture was removed using a rotary evaporator and the product was purified by recrystallization using THF and *n*-hexane as a mixed

solvent system.[42] BLA-NCA, a white powdery substance, was obtained by freeze-drying.

4.2.2.3. Synthesis of folic Acid-poly(ethylene glycol)-poly-(β-benzyl-L-aspartate) copolymers. FA–PEG–PBLA copolymers were prepared by ring-opening polymerization of BLA-NCA. BLA-NCA (1.3651 g; 5.5 mmol) was dissolved in DMF and FA–PEG–NH_2 (415.7 mg; 0.11 mmol) dissolved in chloroform was added. The quantities of solvents were adjusted to 2 ml of DMF per 1 g of BLA-NCA, with chloroform added at 10× the DMF concentration. The reaction was allowed to proceed at 40 °C for 48 h in the dark under nitrogen. The reaction mixture was precipitated with excess cold diethyl ether, and the precipitate was collected by centrifugation. The precipitate was dissolved in 1,4-dioxane and freeze-dried.[43]

4.2.2.4. Introduction of α-lipoic acid to folic Acid-poly(ethylene glycol)-poly(β-benzyl-L-aspartate) copolymers (FA–PEG–PBLA–LA) and removal of the Benzyl groups (FA–PEG–P(Asp-Hyd)–LA). FA–PEG–$PBLA_{50}$ (2.4965 g; 0.18 mmol) was dissolved completely in DMSO (25 ml), then NHS (37 mg; 0.32 mmol), EDC (62.2 mg; 0.32 mmol), LA (55.8 mg; 0.27 mmol), and TEA (170 μl; 2.1 mmol) were added sequentially. The reaction mixture was stirred at 400 rpm for 24 h at room temperature in the dark under nitrogen. Subsequently, the hydrazine monohydrate (6.96 ml; 90 mmol; 10-fold excess of hydrazine monohydrate relative to benzyl groups) was added to substitute the benzyl esters at the side chains of FA–PEG–PBLA with hydrazide groups. The reaction was stirred at 1000 rpm for 4 h at room temperature in the dark, diluted with 5 ml deionized water, and the product was purified by dialysis against deionized water, followed by freeze-drying.[44]

4.2.2.5. Ring opening of FA–PEG–P(Asp-Hyd)–LA (FA–PEG–P(Asp-Hyd)–DHLA). FA–PEG–P(Asp-Hyd)$_{50}$–LA (872.4 mg; 0.084 mmol) was dispersed in 40 ml of deionized water and, after complete dissolution, 8 ml of methanol was added. The flask was sealed, purged with N_2, and put into an ice-bath. 1.6 ml of 10 mg ml^{-1} sodium borohydride aqueous solution was slowly injected into the reaction mixture. The reaction mixture was stirred at 400 rpm for 2 h in the ice-bath. Then, the reaction mixture was warmed to room temperature and left to stir for 12 h.[14] The reaction mixture was centrifuged and the supernatant was purified by dialysis against deionized water followed by freeze-drying.

4.2.3. Surface modification of AuNPs using FA–PEG–P(Asp-Hyd)–DHLA. The ligand cap exchange method was used to modify the FA–PEG–P(Asp-Hyd)–DHLA polymeric ligands onto the surface of citrate-stabilized AuNPs. It has been known that following ring opening of the terminal dithiolane to produce a dithiol group, the resulting dihydrolipoic acid appended ligands allowed effective cap exchange of the citrate-stabilized AuNPs.[14,15] FA–PEG–P(Asp-Hyd)$_{50}$–DHLA (100 mg; 9.6×10^{-3} mmol) was dissolved in 16 ml deionized water and the solution pH was adjusted to 10 by adding 0.5 M NaOH solution. The FA–PEG–P(Asp-Hyd)$_{50}$–DHLA solution was added into 150 ml (1.98×10^{-9} mmol ml^{-1}) of citrate-stabilized AuNP solution. The mixture was stirred at 600 rpm for 24 h at room temperature in the dark. The FA–PEG–P(Asp-Hyd)$_{50}$–DHLA modified AuNP products were purified by dialysis against deionized water for 4 h, and then freeze-dried.

4.2.4. PS conjugation onto FA–PEG–P(Asp-Hyd)$_{50}$–DHLA-modified AuNPs

4.2.4.1. Modification of Pheo. After Pheo (104.3 mg; 0.176 mol) was dissolved completely in methanol (30 ml), EDC (101.3 mg; 0.53 mmol), DMAP (64.7 mg; 0.53 mmol), and 4-hydroxy-2-butanone (120 μl; 1.39 mmol) were added to the Pheo solution. The reaction mixture was stirred at 400 rpm for 24 h at room temperature in the dark. The solvent was removed *via* a vacuum oven, and the residue was washed with deionized water several times. The product was collected by centrifugation until the supernatant was colorless, and then freeze-dried.

4.2.4.2. Conjugation of Pheo to modified AuNPs through a pH-sensitive linkage. FA–PEG–P(Asp-Hyd)$_{50}$–DHLA-modified AuNPs (90 mg; 8.3×10^{-3} mmol) were dissolved in DMSO (8 ml). Modified Pheo (30 mg; 0.05 mmol) dissolved in DCM (4 ml) was slowly added into the FA–PEG–P(Asp-Hyd)$_{50}$–DHLA–AuNPs solution. Subsequently, four drops of acetic acid were added into the mixture. The reaction mixture was stirred at 500 rpm for 24 h at room temperature in the dark. After the reaction, the DCM was removed under vacuum, and then 32 ml of DMSO was added into the residue to adjust the concentration of the mixture to about 3 mg ml^{-1}. After mixing, the solution was dialyzed against $NaHCO_3$ (pH 8.0) solution for 1 day, and then against deionized water for another 12 h. Then the product was centrifuged to remove unreacted Pheo, and the product was freeze-dried and analyzed by ^1H NMR spectroscopy.

4.3. Characterization of Au-based nanoparticles

The compositions and molecular weights of the copolymers were determined by 400 MHz ^1H NMR (JNM-AL400, JEOL, Tokyo, Japan) using D_2O, DMSO-d_6 as the solvent. The sizes and size distributions of the nanoparticles were determined by dynamic light scattering (DLS) (ELS-Z, OTSUKA, Japan) at 25 °C using a He–Ne laser (633 nm) as a light source. The scattered light was measured at 90° and collected by the autocorrelator. The surface modification of AuNPs was confirmed by UV-visible spectrophotometry (UVmini-1240, Shimadzu, Japan), FT-IR spectrometry (FTS-175C, Bio-Rad Laborartories, Inc., Cambridge, USA) and X-ray photoelectron spectroscopy (XPS) (MultiLab 2000, Thermo, Massachusetts, USA). Since the powder form of the citrate-stabilized AuNPs sample was difficult to obtain, the citrate-stabilized AuNPs solution was coated on a silicon wafer and used for XPS analysis. FA–PEG–P(Asp-Hyd)$_{50}$–DHLA–AuNPs and FA–PEG–P(Asp-Hyd)$_{50}$–DHLA–AuNPs–Pheo powder samples were detected directly. The morphologies of the nanoparticles were determined by field emission scanning electron microscopy (FE-SEM) (Magellan400, FEI, Oregon, USA) and field emission transmission electron microscopy (FE-TEM) (Tecnai F20, Philips, Amsterdam, Netherlands). The morphology of AuNPs in HeLa cells was determined by Bio-transmission electron microscopy (Bio-TEM) (Tecnai G^2 Spirit, FEI, Oregon, USA).

4.4. Stability of Au-based nanoparticles

After FA–PEG–P(Asp-Hyd)$_{50}$–DHLA modification, the stability of the AuNPs under a series of harsh conditions, such as mixing

with 0.1 M NaCl solution, mixing with phosphate buffered saline (PBS), and the dialysis process was determined. The nanoparticle stability in both acidic and basic conditions also was determined; the pH value was adjusted by adding 2 M NaOH solution or acetic acid. Under various conditions, the photographs of AuNPs and FA–PEG–P(Asp-Hyd)$_{50}$–DHLA–AuNPs were taken, and the properties of the solution were determined by UV-visible spectrophotometry (UVmini-1240, Shimadzu, Japan).

4.5. Cellular uptake of FA–PEG–P(Asp-Hyd)$_{50}$–DHLA–AuNPs–Pheo and CH$_3$–PEG–P(Asp-Hyd)$_{50}$–DHLA–AuNPs–Pheo

To verify the folic acid effect on cellular uptake, a folic acid unconjugated block copolymer CH$_3$–PEG–P(Asp-Hyd)$_{50}$–DHLA was synthesized using a similar method as a control. It has similar physicochemical characteristics (particle size, *in vitro* stability, morphology, and drug conjugation contents) compared to FA–PEG–P(Asp-Hyd)$_{50}$–DHLA, as shown in Table 1.

HeLa cells (1×10^5 cells per well) were seeded onto 6-well plates and cultured in RPMI 1640 containing 10% FBS, and 1% penicillin–streptomycin at 37 °C in a humidified 5% CO_2–95% air atmosphere. After 24 h, the medium was replaced with 1.5 ml of fresh medium containing free Pheo (10 μg ml^{-1}), FA–PEG–P(Asp-Hyd)$_{50}$–DHLA–AuNPs–Pheo (90 μg ml^{-1}), or CH$_3$–PEG–P(Asp-Hyd)$_{50}$–DHLA–AuNPs–Pheo (100 μg ml^{-1})(10 μg ml^{-1} Pheo equiv.), and then incubated for 4 h. The cells were then washed with PBS and harvested using 0.05% trypsin–EDTA. 4′,6-Diamidine-2-phenylindole (DAPI) and Alexa Fluor 488 phalloidin solutions were added to stain the cell nucleus and F-actin, respectively, at room temperature. All experiments were carried out in a dark room to prevent photodegradation of the probes. The cells were visualized using a Zeiss LSM 510 confocal laser scanning microscope (Carl Zeiss Ltd, Germany).

For the flow cytometry assay, HeLa cells (1×10^5 cells per well) were seeded onto 6-well plates in 1.5 ml RPMI 1640 and allowed to attach for 24 h. After cell attachment, the medium was replaced with 1.5 ml of fresh medium containing free Pheo (10 μg ml^{-1}), FA–PEG–P(Asp-Hyd)$_{50}$–DHLA–AuNPs–Pheo (90 μg ml^{-1}), or CH$_3$–PEG–P(Asp-Hyd)$_{50}$–DHLA–AuNPs–Pheo (100 μg ml^{-1}) (10 μg ml^{-1} Pheo equiv.), and then incubated for 4 h. The cells were then washed with PBS and trypsinized. The harvested cells were washed by cold PBS and fixed using 4% paraformaldehyde solution. After fixation, the sample was washed again using PBS, and then the cellular fluorescence was quantified by FACSCAN flow cytometry (BD Biosciences, USA). The Pheo fluorescence was excited by a laser at 670 nm.

4.6. Monitoring cellular uptake of AuNPs with TEM

HeLa cells (1×10^5 cells per well) were seeded onto 6-well plates in 1.5 ml RPMI 1640 and allowed to attach for 24 h. After cell attachment, the medium was replaced with 1.5 ml of fresh medium containing FA–PEG–P(Asp-Hyd)$_{50}$–DHLA–AuNPs–Pheo (1 mg ml^{-1}), and then incubated for 24 h. Then the cells were washed with PBS and fixed in 2.5% glutaraldehyde for 1 h. After several PBS washes, the samples were stained with 2% osmium tetroxide and 0.5% uranyl acetate. The samples were gradually dehydrated in ethanol and embedded in Epon–propylene oxide. Briefly, the samples were dehydrated with a concentration series of ethanol (30, 50, 70, 80, 90, 95, 99, and 100%; 40 seconds per change). Propylene oxide (PO) was added in PO–ethanol solutions at ethanol–PO = 50 : 50, ethanol–PO = 25 : 75, and PO 100%. Then, Epon–PO was added, and the samples were held at 40 °C overnight. Thin sections were obtained with an ultramicrotome and deposited onto TEM grids. The images were taken on a Bio-TEM.

4.7. *In vitro* phototoxicity test of Pheo-conjugated nanoparticles

HeLa cells (1×10^4 cells per well) were seeded onto 6-well plates in 1.5 ml RPMI 1640 and allowed to attach for 24 h. After cell attachment, the medium was replaced with 1.5 ml of fresh medium containing free Pheo (10 μg ml^{-1}), FA–PEG–P(Asp-Hyd)$_{50}$–DHLA–AuNPs–Pheo (90 μg ml^{-1}), or CH$_3$–PEG–P(Asp-Hyd)$_{50}$–DHLA–AuNPs–Pheo (100 μg ml^{-1})(10 μg ml^{-1} Pheo equiv.), and then incubated for 4 h. The cells were washed with PBS and replaced with fresh culture medium. The samples were irradiated at 0.4 mW cm^{-2} with a He–Ne laser (670 nm) for 0, 15, and 30 min. Then, irradiated cells were incubated at 37 °C for 24 h and cell viability was evaluated by Cell Counting Kit 8 (CCK-8, Dojindo Laboratories, Japan). Untreated cells served as 100% viable cells. Dark-toxicity of FA–PEG–P(Asp-Hyd)$_{50}$–DHLA–AuNPs–Pheo was also evaluated by incubating for 4 h at the same Pheo concentration without laser irradiation. To determine the effect of Pheo concentration on the phototoxicity, we also investigated the *in vitro* phototoxicity of free Pheo and FA–PEG–P(Asp-Hyd)$_{50}$–DHLA–AuNPs–Pheo under a series of concentrations (0, 3, 6, 10, 15, and 20 μg ml^{-1}, Pheo equiv.) with laser treatment at 0.4 mW cm^{-2} for 10 min.

Acknowledgements

This research was supported by Basic Science Research Program through the National Research Foundation of Korea (NRF) funded by the Ministry of Education, Science and Technology (NRF-2012R1A1A3013658).

References

1 J. R. McCarthy, *Adv. Drug Delivery Rev.*, 2010, **62**, 1023.
2 B. Sumer and J. M. Gao, *Nanomedicine*, 2008, **3**, 137.
3 J. Funkhouser, *Curr. Drug Discovery*, 2002, **2**, 17.
4 S. S. Kelkar and T. M. Reineke, *Bioconjugate Chem.*, 2011, **22**, 1879.
5 R. Ackroyd, C. Kelty, N. Brown and M. Reed, *Photochem. Photobiol.*, 2001, **74**, 656.
6 T. J. Dougherty, C. J. Gomer and B. W. Henderson, *J. Natl. Cancer Inst.*, 1998, **90**, 889.
7 B. C. Wilson, *Can. J. Gastroenterol.*, 2002, **16**, 393.
8 T. J. Dougherty, *Photochem. Photobiol.*, 1987, **45**, 879.
9 R. R. Allison, R. E. Cuenca, G. H. Downie, P. Camnitz, B. Brodish and C. H. Sibata, *Photodiagn. Photodyn. Ther.*, 2005, **2**, 205.

10 M. C. DeRosa and R. J. Crutchley, *Coord. Chem. Rev.*, 2002, **233–234**, 351.
11 B. Kim, G. Han, B. J. Toley, C. K. Kim, V. M. Rotello and N. S. Forbes, *Nat. Nanotechnol.*, 2010, **5**, 465.
12 E. C. Dreaden, A. M. Alkilany, X. H. Huang, C. J. Murphy and M. A. E. Sayed, *Chem. Soc. Rev.*, 2012, **41**, 2740.
13 H. Elnakat and M. Ratnam, *Adv. Drug Delivery Rev.*, 2004, **56**, 1067.
14 B. C. Mei, K. Susumu1, I. L. Medintz and H. Mattoussil, *Nat. Protoc.*, 2009, **4**, 412.
15 E. Oh, K. Susumu, J. B. B. Canosa, I. L. Medintz, P. E. Dawson and H. Mattoussi, *Small*, 2010, **6**, 1273.
16 H. Shmeeda, L. Mak, D. Tzemach, P. Astrahan, M. Tarshish and A. Gabizon, *Mol. Cancer Ther.*, 2006, **5**, 818.
17 H. Elnakat and M. Ratnam, *Adv. Drug Delivery Rev.*, 2004, **56**, 1067.
18 M. Geszke, M. Murias, L. Balan, G. Medjahdi, J. Korczynski, M. Moritz, J. Lulek and R. Schneider, *Acta Biomater.*, 2011, **7**, 1327.
19 Y. S. Bae, N. Nishiyama, S. Fukushima, H. Koyama, M. Yasuhiro and K. Kataoka, *Bioconjugate Chem.*, 2005, **16**, 122.
20 G. Gaucher, M. H. Dufresne, V. P. Sant, N. Kang, D. Maysinger and J. C. Leroux, *J. Controlled Release*, 2005, **109**, 169.
21 M. C. Jones and J. C. Leroux, *Eur. J. Pharm. Biopharm.*, 1999, **48**, 101.
22 A. A. Kale and V. P. Torchilin, *Bioconjugate Chem.*, 2007, **18**, 363.
23 I. P. Huang, S. P. Sun, S. H. Cheng, C. H. Lee, C. Y. Wu, C. S. Yang, L. W. Lo and Y. K. Lai, *Mol. Cancer Ther.*, 2011, **10**, 761.
24 K. R. West and S. Otto, *Curr. Drug Discovery Technol.*, 2005, **2**, 123.
25 Y. Cheng, A. C. Samia, J. Li, M. E. Kenney, A. Resnick and C. Burda, *Langmuir*, 2010, **26**, 2248.
26 Y. Cheng, A. C. Samia, J. D. Meyers, I. Panagopoulos, B. Fei and C. Burda, *J. Am. Chem. Soc.*, 2008, **130**, 10643.
27 T. Stuchinskaya, M. Moreno, M. J. Cook, D. R. Edwardsb and D. A. Russell, *Photochem. Photobiol. Sci.*, 2011, **10**, 822.
28 L. Zhao, T. H. Kim, K. M. Huh, H. W. Kim and S. Y. Kim, *J. Biomater. Appl.*, 2013, **28**, 434.
29 Y. L. Liu, M. K. Shipton, J. Ryan, E. D. Kaufman, S. Franzen and D. L. Feldheim, *Anal. Chem.*, 2007, **79**, 2221.
30 K. E. Schmalenberg, L. Frauchiger, L. N. Albers and K. E. Uhrich, *Biomacromolecules*, 2001, **2**, 851.
31 K. Nawalany, A. Rusin, M. Kepczynski, A. Mikhailov, G. K. Marek, M. Snietura, J. Poltowicz, Z. Krawczyk and M. Nowakowska, *J. Photochem. Photobiol., B*, 2009, **97**, 8.
32 P. Nativo, I. A. Prior and M. Brust, *ACS Nano*, 2008, **2**, 1639.
33 F. Zhao, Y. Zhao, Y. Liu, X. L. Chang, C. Y. Chen and Y. L. Zhao, *Small*, 2011, **7**, 1322.
34 C. J. Murphy, A. M. Gole, J. W. Stone, P. N. Sisco, A. M. Alkilany, E. C. Goldsmith and S. C. Baxter, *Acc. Chem. Res.*, 2008, **41**, 1721.
35 N. Lewinski, V. Colvin and R. Drezek, *Small*, 2008, **4**, 26.
36 A. A. Krasnovsky, K. V. Neverov and S. Y. Egorov, *J. Photochem. Photobiol., B*, 1990, **5**, 245.
37 G. Frens, *Nature*, 1973, **241**, 20.
38 W. Haiss, N. T. K. Thanh, J. Aveyard and D. G. Fernig, *Anal. Chem.*, 2007, **79**, 4215.
39 H. S. Yoo and T. G. Park, *J. Controlled Release*, 2004, **96**, 273.
40 H. Z. Zhao and L. Y. L. Yung, *Int. J. Pharm.*, 2008, **349**, 256.
41 R. J. Lee and P. S. Low, *Biochim. Biophys. Acta*, 1995, **1233**, 134.
42 M. Prabaharan, J. J. Grailer, S. Pilla, D. A. Steeber and S. Q. Gong, *Biomaterials*, 2009, **30**, 5757.
43 M. Yokoyama, G. S. Kwon, T. Okano, Y. Sakurai, T. Seto and K. Kataoka, *Bioconjugate Chem.*, 1992, **3**, 295.
44 K. Akamatsu, Y. Yamasaki, M. Nishikawa, Y. Takakura and M. Hashida, *J. Pharmacol. Exp. Ther.*, 1999, **290**, 1242.